Eco-Friendly Photodegradation and Anti-bacterial Treatment of Dye Effluents with special reference to Malachite Green using $SrFe_{12}O_{19}$ /TiO_2 /ZnO Ternary Nanocomposites

Ramya Kumari Ch[1*], Jyothi Priya K[1], Suneetha M[1], Sridevi Chandrakala N[1], Bulli Babu T[1], Padma M[1] and Paul Douglas S[1*]

[1]Department of Engineering Chemistry, Andhra University College of Engineering [A], Andhra University, Visakhapatnam-530003, Andhra Pradesh, INDIA
*Mobile: + 91 9908534256; +91 9347098430
*Email: ramyametta99@gmail.com; spdfchem@andhrauniversity.edu.in

Abstract. A novel ternary metal oxide nanocomposite ($SrFe_{12}O_{19}$/TiO_2/ZnO) was synthesized using the sol-gel method for malachite green dye degradation. The absorption maximum was determined by ultraviolet-diffuse reflectance spectroscopy (DRS), revealing a bandgap of 2.29 eV. Fourier transform infrared spectroscopy (FT-IR) confirmed the formation of metal-oxygen bonds, indicating the presence of functional groups in the fabricated metal oxides. The average crystallite size was calculated to be around 30 nm based on X-ray powder diffraction (XRD) analysis. Structural properties, phase purity, and surface morphology were examined using scanning electron microscopy (SEM), while high-resolution transmission electron microscopy (HR-TEM) showed a spherical morphology. The elemental composition was determined via energy-dispersive X-ray analysis (EDAX), and magnetic properties were studied through vibrating sample magnetometry (VSM). The nanocomposite exhibited 100% degradation of malachite green dye Lambda max – 917 nm at a 10-ppm concentration, pH-8 under visible light, demonstrating superior photocatalytic activity compared to pure magnetite and $SrFe_{12}O_{19}$/TiO_2/ZnO. This enhanced efficiency is attributed to the synergistic interaction between TiO_2, ZnO, and $SrFe_{12}O_{19}$, which improves charge separation, light absorption, and the generation of reactive oxygen species (ROS), promoting pollutant degradation. Antibacterial tests against Gram-negative Salmonella enterica (ATCC no: 35664) and Gram-positive Mycobacterium tuberculosis (ATCC no. 25618/H37RV) revealed potent activity, with the nanocomposite reusable for up to three cycles.

R. K. Ramachandra et al. (eds.), *Proceedings of the International Conference on Bio-Based Environment for Sustainable Territory (IC-BEST 2024)*, Advances in Biological Sciences Research 44,
https://doi.org/10.2991/978-94-6463-648-2_18

Therefore, this highly efficient, cost-effective, and reusable catalyst is suitable for removing toxic organic pollutants from industrial wastewater.

Keywords: $SrFe_{12}O_{19}/ZnO/TiO_2$ nanomagnetic composites, Visible-light Photodegradation, Malachite Green dye.

1. Introduction: A major environmental challenge today is wastewater pollution, as large amounts of synthetic contaminants such as pharmaceuticals, antibiotics, dyes, pesticides, and personal care products enter natural waters through industrial and residential wastewater [1]. Clean water is essential for life, but contamination now threatens ecosystems globally. Industrial activities like power plants, mining, and climate-related disasters have spread harmful chemicals in water bodies. In many areas, pollution and population growth have created a severe shortage of safe drinking water [2]. Previous efforts to improve methods like natural aerobic treatment, coagulation, membrane filtration, and adsorption were limited by complexity, cost, and sludge issues. In contrast, advanced oxidation processes (AOPs) are highly effective for wastewater treatment, using photocatalytic oxidation to decompose organic pollutants. Photocatalytic reactions, driven by light and a catalyst, provide benefits like full pollutant breakdown, environmental protection, and no secondary pollution [3]. Advanced oxidation processes (AOPs) hold strong potential for removing emerging pollutants from wastewater. Photocatalysis, a widely researched AOP, has seen over 32,500 publications on photocatalysis and water in the past 20 years, with yearly growth indicating sustained interest and progress in sustainable methods. This research surge parallels extensive studies on the structural properties and physicochemical of photoactive materials used in cancer treatment, self-cleaning surfaces, wastewater treatment, and air purification [4]. Photocatalytic degradation offers a cost-effective and efficient approach for breaking down dye molecules this process, when light is absorbed by a photocatalyst, Electron-hole pairs are formed when electrons migrate from the valence band to the conduction band. Following their reaction with water, these pairs create hydroxyl radicals, quickly breaking down organic pigments and transforming them into gases like CO_2 and H_2O. [5]. Heterogenous catalysis, where a solid catalyst interacts with gas or solid or liquid reactants begins with reactant adsorption on the catalyst surface increasing their concentration and aiding activation. The reaction involves energy barriers for adsorbing reactants (A_{ads}), forming intermediates (I_{ads}), and desorbing products (P_{ads}). The catalytic efficiency depends on the energy needed at each step adsorption, intermediate formation, and product release [6]. The gigahertz range is effectively absorbed by M-type hexaferrites, $MFe_{12}O_{19}$ (where M might be Ba, Sr, or Pb), because of their mild saturation magnetization, high resistivity, and significant anisotropy field. Recent studies indicate that particle morphology, size, and Fe^{3+} ion substitution play important roles in influencing microwave absorption. Composites made of both dielectric and magnetic materials improve microwave absorption by combining dielectric loss from materials like $BaTiO_3$, ZnO, SiC, and conductive polymers with magnetic loss from magnetic components [7]. Known for their strong hard magnetic characteristics, hexagonal strontium ferrite ($SrFe_{12}O_{19}$) nanoparticles are valuable for their affordability, excellent magneto-crystalline anisotropy, and high boiling point. Research on Sono chemical synthesis has investigated their effectiveness in adsorbing malachite green dye and their antibacterial potential [8]. Adjusting the material's magnetic permeability and dielectric permittivity and adding dielectric and magnetic fillers are crucial for optimizing electromagnetic radiation absorption. Particularly helpful is TiO_2, which increases infrared absorption without increasing electromagnetic radiation since it is transparent and stable at microwave wavelengths [9]. Nanostructured adsorbents like manganese, titanium, iron, and zinc oxides are effective for heavy metal removal, with zinc oxide (ZnO) particularly suitable for organic and inorganic pollutants despite some technical challenges. ZnO nanoparticles are prized for their optical, electrical, and antimicrobial properties, finding applications in rubber, plastics, cosmetics, pharmaceuticals, electronics, and biomedical devices. ZnO's demand is rising, and it is also studied for water treatment, adsorbing heavy metals like Cu (II), Cr (VI), Cd (II), and Pb (II).[10]. It is commonly known that the photodecomposition phenomenon causes TiO_2 and ZnO to lose their photocatalytic activity when they come into direct contact with magnetic cores. [11]. The benefit of using chemical processes is that they can produce particles with exact size, shape, composition, and structure. which is ideal for catalysis, sensing, and electronics. Additionally, methods like the sol-gel process are more cost-effective because they operate at lower temperatures and require less energy as compared with physical methods. Nanoparticle shape and size greatly impact their properties [12]. Organic dyes are typically toxic, carcinogenic, mutagenic, and highly stable. The cationic dye Malachite Green (MG) is particularly notable for its high solubility in water [13]. Because of its physicochemical characteristics, malachite green (MG) is a dye that should be used. Leather, silk, cotton, jute, paper, and other materials can all be colored using it. In addition to coloring leather, jute, paper, cotton, silk, and wool, it is also used for food. color. Additionally, MG is an antiseptic and fungicide in aquaculture and an anthelminthic and disinfectant in medicine. However, MG is persistent and can bioaccumulate in aquatic organisms, potentially entering the human food chain. It poses toxic risks, including carcinogenic, teratogenic, and mutagenic effects. In mammals, MG can be reduced to leucomalachite green (LMG), which may persist in the body for over five months and has been linked to lung adenomas in rats and liver tumors under certain conditions [14]. This study explores the degradation of organic dyes in water and wastewater using magnetic ferrite-based nanocomposites of titanium oxide and zinc oxide. While various studies have examined ferrite-based photocatalysts for wastewater treatment, Extensive studies of their application in combined photocatalytic technologies appeared insufficient. Here, we used the sol-gel approach to create trimetallic nanocomposites ($SrFe_{12}O_{19}$-ZnO-TiO_2) from their corresponding precursor components. X-ray diffraction (XRD) and scanning electron microscopy (SEM) were used to analyze the nanocomposites. Under solar radiation, the produced nanocomposites were employed as photocatalysts to break down Malachite Green dye repetitively used in the textile, dyeing, and pharmaceutical industries

2. Materials and Methods:

The chemicals used in this study included zinc nitrate, ethylene glycol, strontium nitrate, ferric citrate, citric acid, titanium tetrachloride, and hydrochloric acid

2.1 Synthesis of Strontium ferrite: 4.23 g of strontium nitrate and 10 mL of distilled water should be dissolved in a single beaker to make a ferric citrate solution. Put 10 mL of water and 71.64 g of ferric citrate in a different beaker. Mix the contents of both beakers with 12.6 g of citric acid. Gradually add ammonia to maintain the solution at a neutral pH. Then, incorporate 20 mL of ethylene glycol into the mixture and use a hot plate to evaporate the liquid, yielding a dry powder. After calcining the mixture at 800 °C for two hours, finely powdered nano strontium ferrite is obtained.

2.2 Synthesis of Titania Nano Composites: A white precipitate was formed by gradually adding 6.9 mL of $TiCl_4$ to a beaker containing 0.5 mL of hydrochloric acid solution and 350 mL of distilled water. The beaker is covered with aluminum foil to shield the reaction from light. After the precipitate formed, the mixture was stirred for one hour. It was then heated on a hot plate at a temperature between 80 °C to 100 °C with continuous stirring, resulting in the production of fine nano titania powder [15].

2.3 Synthesis of Zinc Oxide Nano Composites: Five grams of zinc nitrate and twenty milliliters of ethylene glycol were combined and stirred for an hour to make a uniform solution. After that, this mixture was allowed to gel for a day at room temperature. After being heated on a hot plate, the gel was crushed and allowed to dry. Ultimately, the substance was calcined for two hours at 500 °C, producing finely powdered nano zinc oxide**.**

2.4 Synthesis of $SrFe_{12}O_{19}$/ TiO_2/ ZnO ternary nanocomposites: Ternary nanocomposites were synthesized by combining 0.8 g of $SrFe_{12}O_{19}$, 0.1 g of TiO_2, and 0.1 g of ZnO. These components were accurately weighed and thoroughly mixed using a mortar and pestle to create a homogeneous powder.

2.5 Instrumentation: The resulting materials were analyzed using infrared spectroscopy in the range of 500–4000 cm with the IR PRESTIGE 21. The X-ray diffraction (XRD) pattern was generated using a diffractometer, scanning samples from the BRUKER DX-5 in the angular range of 10-80° (2 theta). The UV–DRS spectra were recorded using a SHIMADZU 2600R, with barium sulfate as a reference, also in the 500–4000 cm range. The morphology and microstructure were examined using a Zeiss Germany 300 scanning electron microscope.

3. Results and Discussion:

3.1. UV-DRS:

Figure 1. shows the results of the UV diffuse reflectance spectroscopy (UV-DRS) study of the magnetic material $SrFe_{12}O_{19}/TiO_2/ZnO$ nanocomposite. The nano strontium ferrite has the greatest absorption wavelength at 365 nm, equivalent to a calculated bandgap of 3.3 eV. In contrast, the $SrFe_{12}O_{19}/TiO_2/ZnO$ nanocomposite displays a maximum absorption wavelength at 351 nm, resulting in a reduced bandgap of 2.3 eV. This reduction in bandgap compared to pure strontium ferrite indicates that the nanocomposite has enhanced absorption in the visible light spectrum.

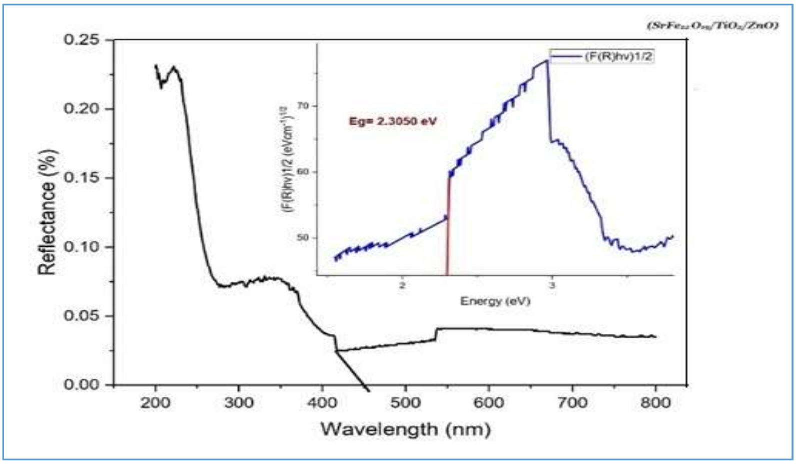

Fig.1 UV-Visible diffuse reflectance spectra $SrFe_{12}O_{19}/TIO_2/ZnO$

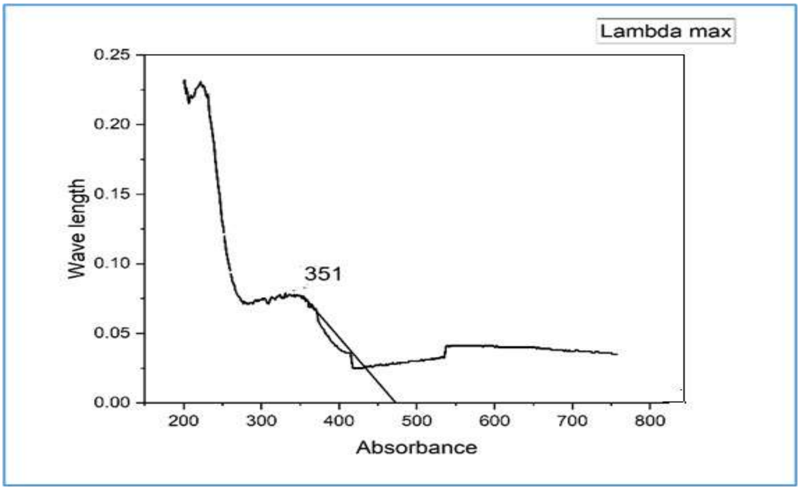

Fig.2 Band gap of $SrFe_{12}O_{19}/TiO_2/ZnO$

3.2. XRD: The X-ray diffraction (XRD) patterns for the $SrFe_{12}O_{19}$ powder and the $SrFe_{12}O_{19}/ZnO/TiO_2$ photocatalytic composite are displayed in the Fig.3 The diffraction peaks match those listed in JCPDS Card No. 79-1411, confirming the presence of the $SrFe_{12}O_{19}$ phase, as well as the anatase TiO_2 phase (JCPDS Card Nos. 21-1272 and 21-1276) and ZnO (JCPDS Card No. 36-1451). The observed 2θ values include 25°, 28°, 29°, 30°, 31°, 32°, 35°, 42°, 45°, 49°, 50°, 55°, 58°, 60°, 65°, 69°, and 70°. Notably, the peaks at 34°, 35°, 56°, and 57° correspond to the (107), (114), and (2011) planes, indicating the presence of strontium ferrite. Additionally, the peaks at 49° and 56° correspond to the (102) and (110) planes, confirming the presence of ZnO, while the peaks at 25° and 55° relate to the (101) and (105) planes, signifying the presence of titanium. The diffractograms exhibit strong peaks, demonstrating the crystallinity of the samples. Thus, the XRD pattern validates the formation of the $SrFe_{12}O_{19}/TiO_2/ZnO$ spinel ferrite composite.

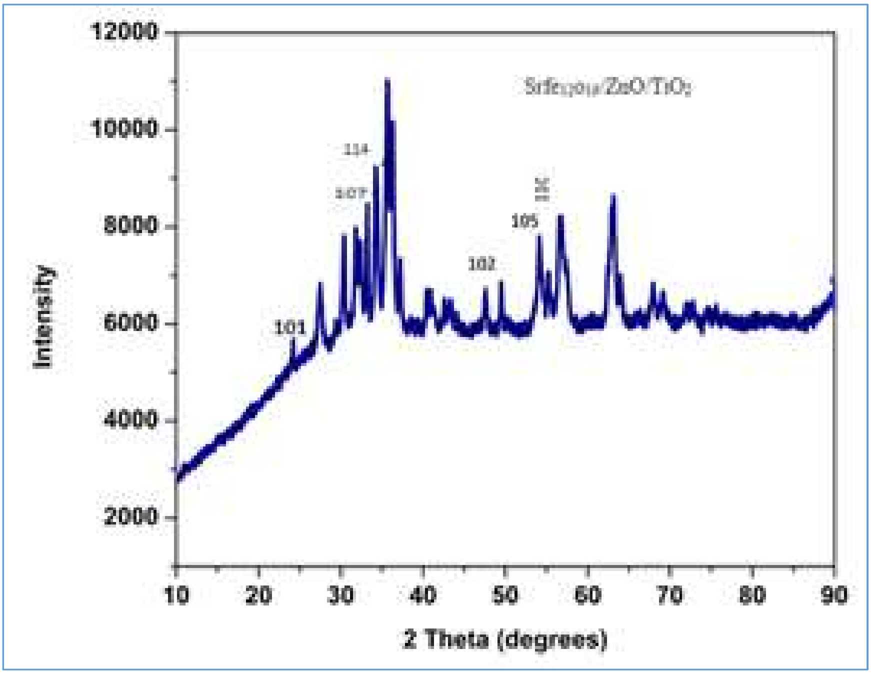

Fig.3 XRD pattern of $SrFe_{12}O_{19}/TiO_2/ZnO$

3.3. SEM Images and EDX analysis: The sizes and morphologies of the resulting $SrFe_{12}O_{19}/TiO_2/ZnO$ ternary nanocomposites were analyzed using scanning electron microscopy (SEM). The SEM images indicate that the diameters of the $SrFe_{12}O_{19}/TiO_2/ZnO$ nanoparticles range from 18 to 50 nm. Observations of pure ZnO nanoparticles reveal that they are relatively large due to the agglomeration of primary particles, exhibiting disc-like and spherical shapes with smooth surfaces. Energy-dispersive spectroscopy (EDS) analysis confirms that these ZnO nanoparticles are composed solely of zinc and oxygen. The SEM micrographs of the $SrFe_{12}O_{19}/TiO_2/ZnO$ nanocomposites display particles with spherical and sheet-like morphologies and rough surfaces. EDS analysis of these nanocomposites, illustrated in the figures and their insets, shows the presence of oxygen, zinc, titanium, strontium, and iron elements. These morphological findings and EDS results align with the

X-ray diffraction (XRD) data, which confirm the purity of the synthesized ternary nanocomposite structure.

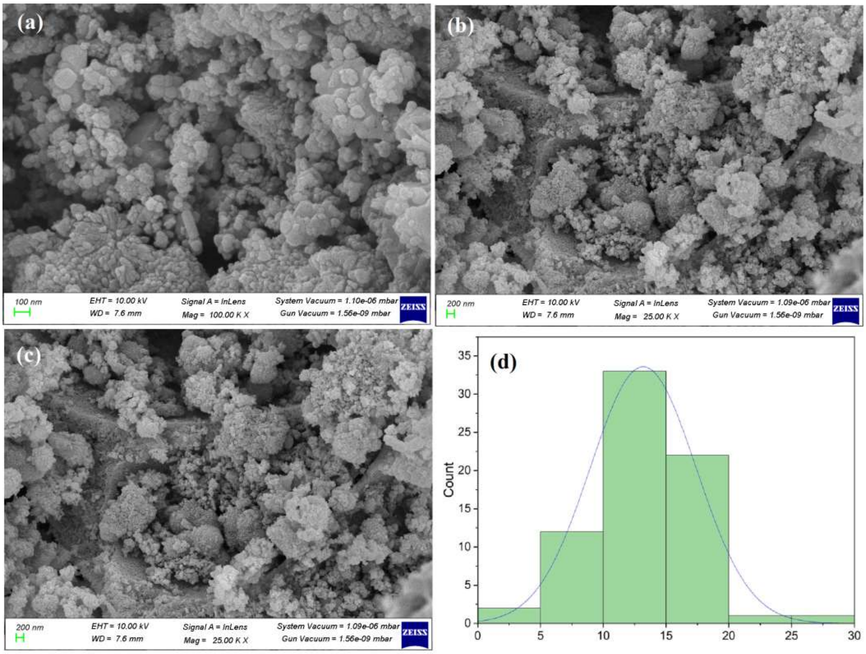

Fig 4.SEM images of $SrFe_{12}O_{19}/TiO_2/ZnO$ (a) 100 nm (b) 200 nm (c) 1µm (d) particle size distribution of $SrFe_{12}O_{19}/TiO_2/ZnO$

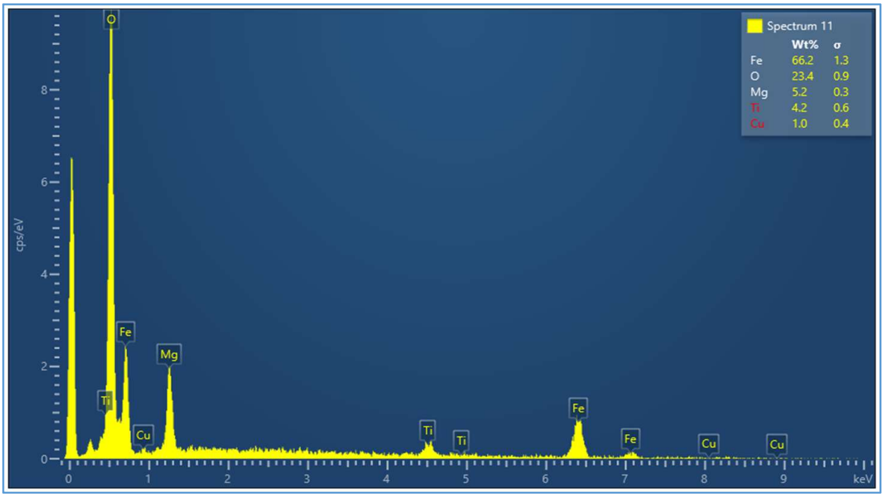

Fig. 5 EDX spectrum of $SrFe_{12}O_{19}/TiO_2/ZnO$

3.4. TEM: The TEM images provided valuable insights into the structure and characteristics of the synthesized materials. The Fig.6 presents a TEM micrograph of the $SrFe_{12}O_{19}/TiO_2/ZnO$ nanoparticles, with an average diameter of 30 nm. The image indicates that these nanoparticles are relatively rough and spherical. Furthermore, the TEM micrograph of $SrFe_{12}O_{19}/TiO_2/ZnO$, as depicted in the figure, shows a similar morphology to the previous image, with the additional observation of a ZnO layer located between the $SrFe_{12}O_{19}$ and TiO_2, as highlighted in the illustration. These observations are consistent with literature reports, confirming the successful integration of the nanoparticles and photocatalyst composites. Additionally, the figure includes a TEM image of the TiO_2 photocatalyst, illustrating the synthesized structure. Following the XRD analysis, it was determined that the TiO_2 photocatalyst primarily consists of elementary particles ranging in size from 15 to 26 nm, which aligns with the findings from the XRD study.

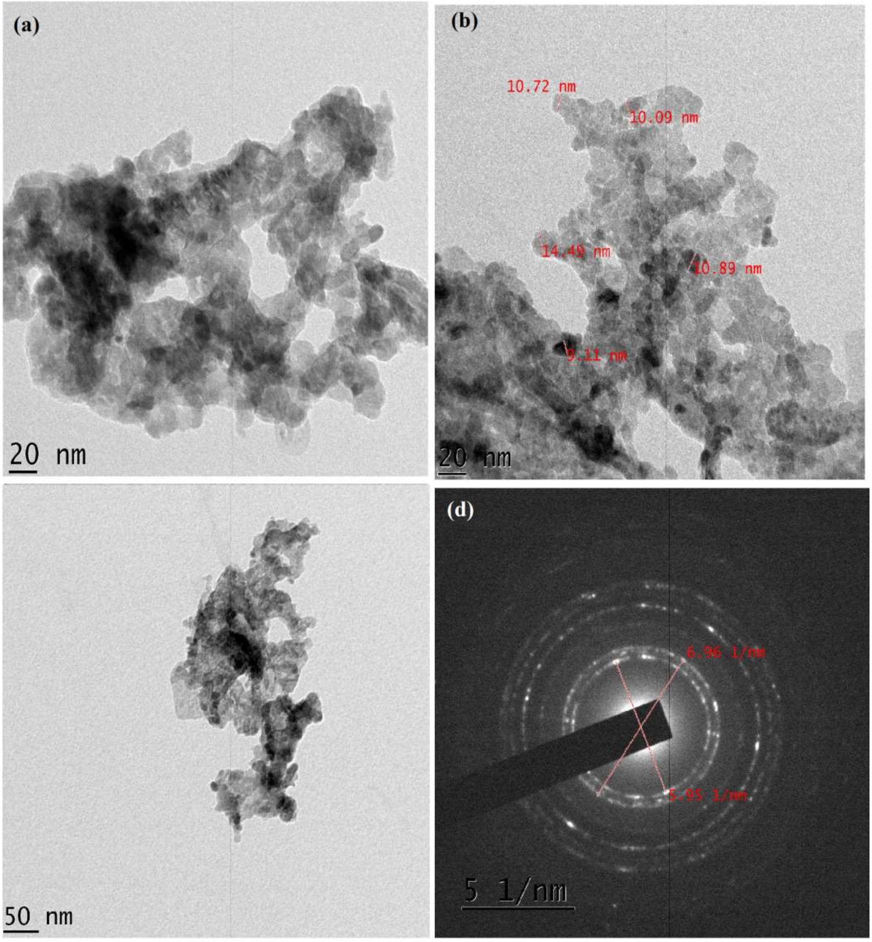

Fig. 6 TEM images of $SrFe_{12}O_{19}/TiO_2/ZnO$ (a) 10 nm (b) 20 nm (c) 50 nm (d) particle size distribution of $SrFe_{12}O_{19}/TiO_2/ZnO$ (TEM)

3.5. FTIR: Fourier transform infrared (FTIR) spectroscopy was used to analyze the $SrFe_{12}O_{19}$ powder and the synthesized photocatalytic composites in greater detail. The FTIR spectrum of $SrFe_{12}O_{19}$ shows peaks between 450 and 493 cm^{-1}, which are recognized as the natural vibrations of the tetrahedral and octahedral sites in its structure The O–H stretching mode of pure water molecules on the surface and the O–H bending vibration of chemically adsorbed water are shown by a peak at 3418 cm^{-1}. $^{-1}$.

Combined with these bands' increased duration and intensity, the $SrFe_{12}O_{19}/ZnO/TiO_2$ composite's shift to lower frequencies suggests a higher concentration of surface hydroxyl groups. The $SrFe_{12}O_{19}/ZnO/TiO_2$ composite may have increased catalytic activity for pollutant removal because these hydroxyl groups serve as active sites for adsorption, hydroxyl radical generation, and oxidative breakdown. Asymmetric stretching vibrations are linked to the absorption peak of the $SrFe_{12}O_{19}/ZnO$ composite, which is approximately 450 cm^{-1}. At 493 cm^{-1}, an asymmetric Ti–O–Zn vibration is also detected, indicating the development of a covalent link between TiO_2 and ZnO. This could enhance TiO_2 adherence to the surface of the $SrFe_{12}O_{19}/ZnO$ composite. Additionally, a peak at 800 cm^{-1}, equivalent to the Ti–O–Ti absorption band, displays a four-fold coordination.

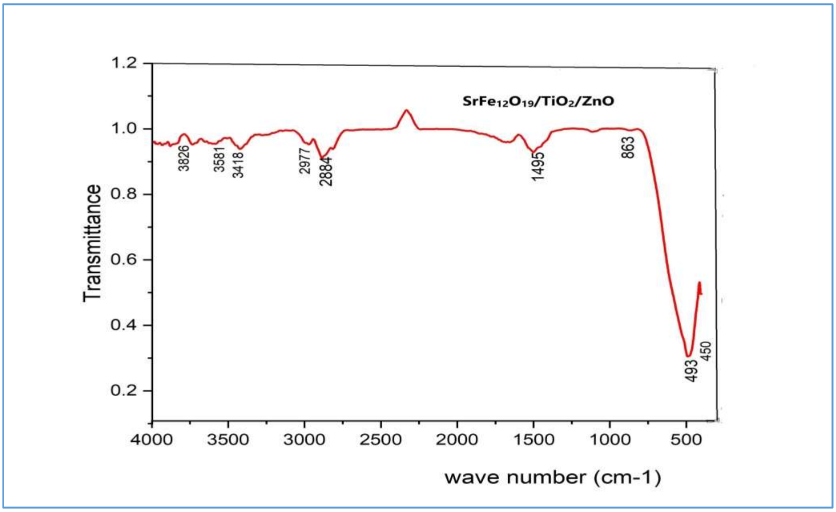

Fig.7 FTIR of $SrFe_{12}O_{19}/TiO_2/ZnO$

3.6. Magnetic Properties: We employed a vibrating sample magnetometer (VSM) to investigate the material's magnetic properties at room temperature. The magnetic characteristics of the synthesized nanocomposite are crucial for its function as a reusable and regenerable magnetic heterogeneous catalyst. The $SrFe_{12}O_{19}/TiO_2/ZnO$ composite exhibits superparamagnetic behavior, with a saturation magnetization of 82 emu/g and nearly zero coercivity. Similarly, magnesium ferrite nanoparticles also display superparamagnetic properties. The inclusion of metal oxides in the composite leads to a reduction in magnetization. This nanocomposite is ideally suited for applications that require the reusable magnetic separation of photocatalytic particles, which helps reduce secondary pollution in water treatment processes. The magnetic hysteresis curve is illustrated in the figure.

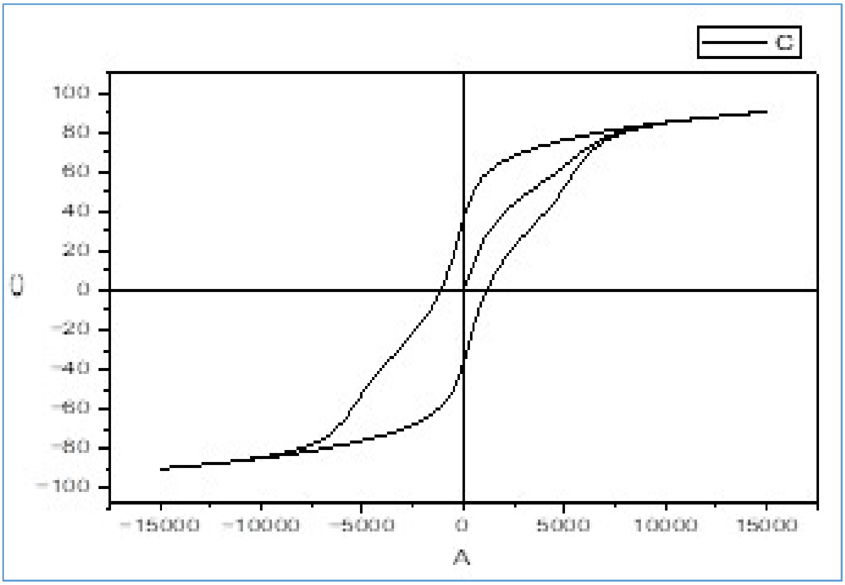

Fig.8 Magnetization loop for $SrFe_{12}O_{19}/ZnO/TiO_2$ composite at room temperature

3.7. Evaluation of Photocatalytic Efficiency of Catalyst Degradation Malachite Green dye: Malachite green dye degradation was utilized to assess the photocatalytic effectiveness of the catalyst. To identify the optimal reaction conditions for enhanced photocatalytic degradation of MG, we investigated the effects of various parameters, including irradiation, temperature, pH, catalyst dose, and initial dye concentration, by systematically varying one parameter while keeping the others constant.

3.7.1. Effect of initial dye concentration: The influence of the initial concentration of Malachite green (MG) dye on the photocatalytic efficiency of the $SrFe_{12}O_{19}/TiO_2/ZnO$ composite was examined by adjusting the dye concentration from 5 mg/L to 100 mg/L while keeping the solution pH at 8 and the catalyst loading at 10 mg/L. The highest degradation rate, achieving 100%, was observed at a concentration of 10 mg/L within 110 minutes. At higher concentrations, the degradation rate decreased due to the "blanket effect," where an excess of MG dye molecules obstructs the active sites on the catalyst surface, thus limiting the generation of hydroxyl (·OH) radicals. Moreover, with the catalyst dosage fixed at 10 mg/L, there was an inadequate supply of reactive species (·OH) to counterbalance the increased number of dye molecules. Another factor that led to a diminished performance at elevated concentrations is the visible light absorption by the dye, which further impedes the photocatalytic reaction.

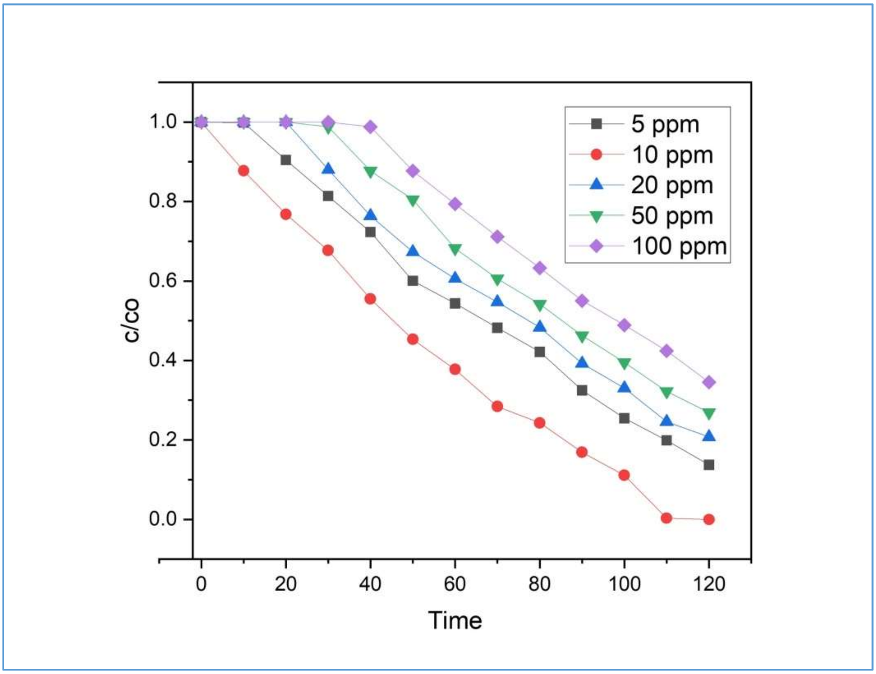

Fig.9 Effect of initial dye concentration on $SrFe_{12}O_{19}/TiO_2/ZnO$

3.7.2. Effect of pH: The pH of the solution influences the photocatalytic degradation of wastewater. To investigate this effect, the pH was adjusted to values between 5 and 8 using 0.1 M HCl and NaOH solutions over 90 minutes.MG was subjected to visible light while other parameters remained constant to evaluate the performance of the $SrFe_{12}o_{19}$ /TiO_2/ZnO nanocomposite. The experimental results, illustrated in the figure, reveal the greatest degradation rate at pH 8.

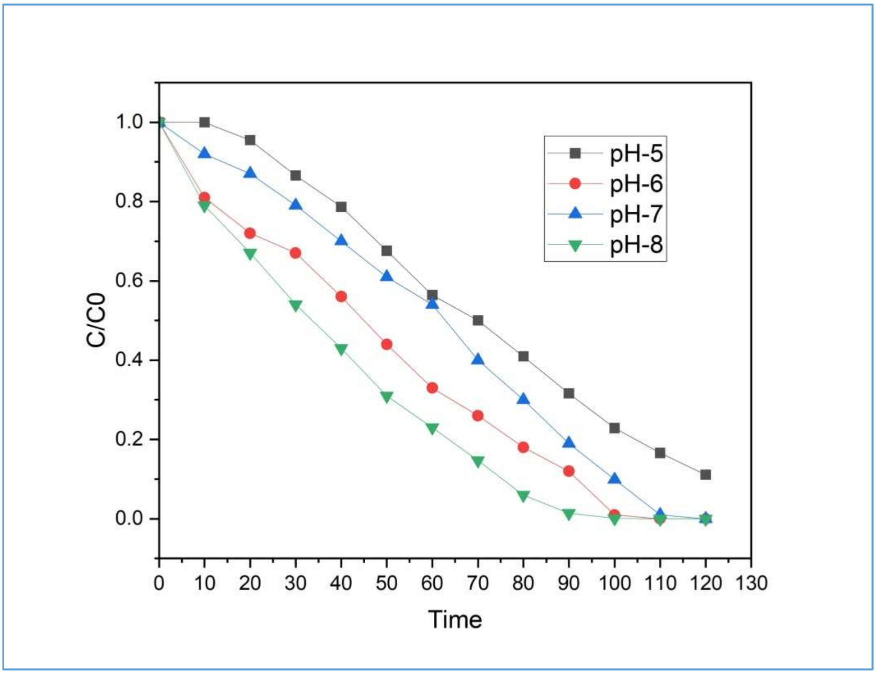

Fig.10. Effect of pH on $SrFe_{12}O_{19}$/TiO_2/ZnO

3.7.3. Effect of Temperature: The influence of adsorption temperature on the removal of MG dye by nanocomposites was investigated within 30 °C to 45 °C. The changes in adsorption percentages over time at various temperatures are depicted in Fig.11. As the temperature rose above 45 °C, the proportion of MG dye adsorbed increased significantly, resulting in complete degradation. The concentration of the dye solution and pH levels were maintained at 10 mg/L and pH 8 respectively. Malachite Green's highest adsorption capacity and efficiency (100%) were recorded at 45 °C after 70 minutes. These findings suggest that the adsorption process is endothermic, indicating that higher temperatures promote enhanced adsorption of MG dye onto the adsorbent, likely facilitating greater dye penetration.

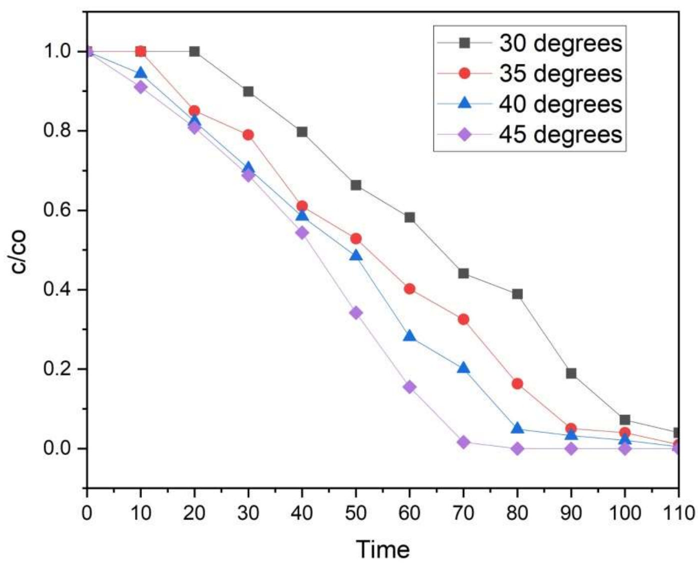

Fig.11. Effect of Temperature on $SrFe_{12}O_{19}/TiO_2/ZnO$

3.7.4. Effect of Catalyst loading: To evaluate the effect of $SrFe_{12}O_{19}/TiO_2/ZnO$ composite concentration on the photocatalytic degradation of malachite green (MG) dye under visible light, the composite concentration was varied from 0.20 g/L to 0.50 g/L, with the solution pH maintained at 8 and the initial dye concentration set at 0.40 g/L. The results, shown in Fig.12, indicate that as the catalyst concentration increased to 0.50 g/L, the degradation rate of MG improved over 50 minutes. However, further increases in catalyst concentration led to a decrease in the degradation rate. This decline may be due to increased turbidity and the agglomeration of catalyst particles, which hinder light penetration and reduce the number of active sites for light absorption. As a result, the photocatalytic activity of the catalyst decreased with higher composite loading.

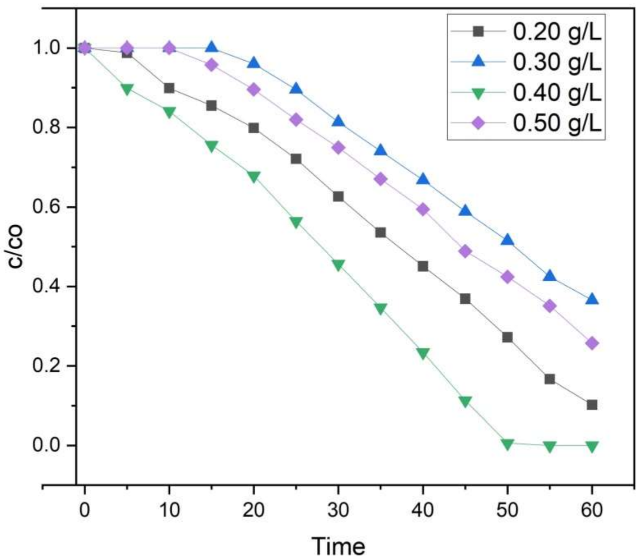

Fig.12. Effect of Catalyst loading on $SrFe_{12}O_{19}/TiO_2/ZnO$

3.7.5. Effect of Irridation; The absorption spectrum of MG dye during solar photocatalysis using $SrFe_{12}o_{19}/TiO_2/ZnO$ catalysts was analyzed. The intensity of the absorption peak at 617 nm gradually decreased as the duration of catalysis increased. Fig.13 presents the photocatalytic degradation efficiency (Ct/C_0 vs. time) for the catalysts evaluated. After 50 minutes, the $SrFe_{12}o_{19}$ $/TiO_2/ZnO$ photocatalysts achieved complete degradation of MG reaching 100% and demonstrating their excellent photocatalytic activity. In contrast, when MG dye was exposed to sunlight without a catalyst, the degradation was significantly lower, underscoring the effectiveness of the developed photocatalyst.

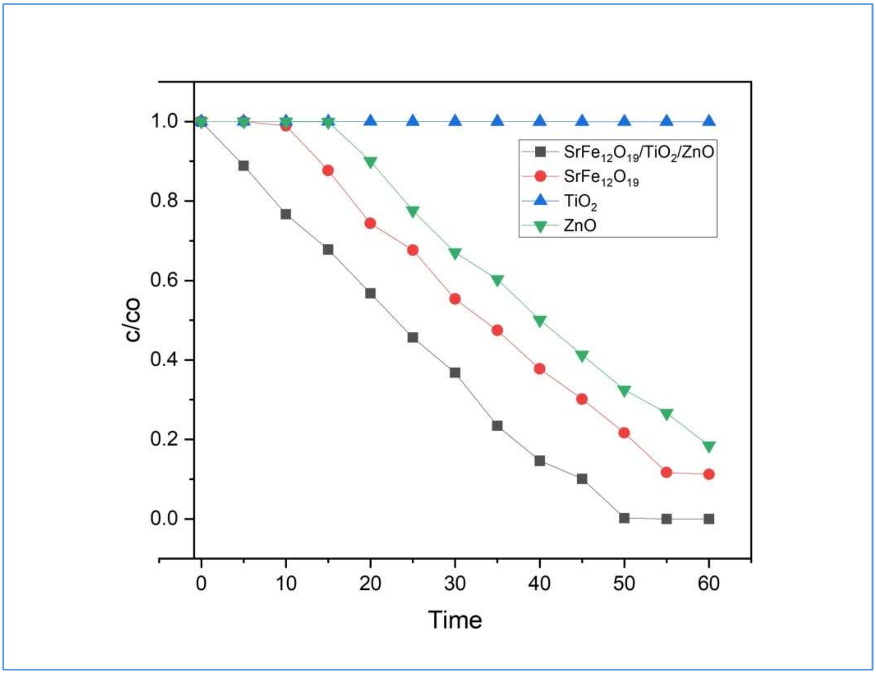

Fig.13.Effect of Irridation on $SrFe_{12}O_{19}/TiO_2/ZnO$

3.7.6. Study on Reusability and Regenerability: Evaluating the reusability of photocatalysts is essential for industrial applications, as it helps reduce costs and ensures environmental safety by minimizing the release of secondary pollutants. The reusability of the photocatalysts was assessed, as illustrated in Fig.14. After each cycle, the photocatalyst was centrifuged, cleaned, and tested for performance over three cycles, demonstrating consistent efficiency. Similarly, as shown in the figure, the photocatalyst maintained high effectiveness over three consecutive cycles of Malachite Green degradation

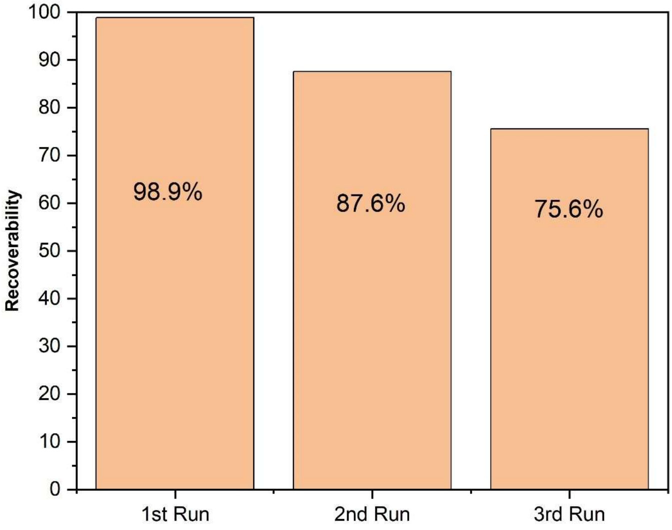

Fig.14. Effect of Reusability on $SrFe_{12}O_{19}/TiO_2/ZnO$

3.8. Antibacterial activity: The test involves placing antimicrobial-impregnated filter paper disks onto the surface of an agar plate inoculated with the patient's microorganism. Upon contact with the agar, the antimicrobial agent begins to diffuse from the disk into the surrounding medium, potentially inhibiting microbial growth. If the antimicrobial agent is effective, a clear zone of inhibition will form around the disk after incubation. The presence or absence of this zone indicates the microorganism's susceptibility to the antimicrobial agent. The Agar well diffusion method assessed the antimicrobial effectiveness of $SrFe_{12}O_{19}/TiO_2/ZnO$. The antibacterial activity was determined by observing the formation of an inhibitory zone around the well. The study focused on both Gram-positive Mycobacterium tuberculosis (ATCC no. 25618/H37RV) and Gram-negative Salmonella enterica (ATCC no: 35664) bacteria. And with Moxifloxacin serving as the standard reference. The inhibitory effect was visible after a 24-hour incubation. Photographs of Petri dishes showing the impact of the different nanomaterials against the bacterial strains indicate that all nanomaterials displayed a significant inhibitory effect on both bacteria. The disc diffusion method evaluated the antibacterial activity of $SrFe_{12}O_{19}/TiO_2/ZnO$ nanocomposites (NCPs). All NCPs effectively inhibited the growth of both Gram-positive Mycobacterium tuberculosis (ATCC no. 25618/H37RV) and Gram-negative Salmonella enterica (ATCC no: 35664) bacteria. Notably, the NCPs showed stronger inhibition against Gram-negative strains, particularly with the composition demonstrating the highest activity. This increased effectiveness against Gram-negative bacteria is due to the structural differences in their cell walls. The thinner cell wall of Gram-negative bacteria allows easier penetration of the nanocomposite particles, forming reactive oxygen species (ROS) within the cell. These ROS then interact with cellular components, damaging material and proteins. The zone of inhibition for each NCP is shown in Fig.15 The table presents the antibacterial activity of two different synthesized nanocomposites, $SrFe_{12}O_{19}/TiO_2/ZnO$ and $SrFe_{12}O_{19}/TiO_2/ZnO$ nanocomposite, compared with the antibiotic Moxifloxacin against two bacterial strains: *Salmonella enterica* (Gram-negative) and *Mycobacterium tuberculosis* (Gram-positive). The antibacterial activity is measured by the zone of inhibition in millimeters (mm) at different concentrations of each sample (in µg/mL). Zones of inhibition for this composite range from 2 to 3 mm, indicating little action against both bacterial strains at lower dosages (10 and 50 µg/mL). But when the concentration is increased to 100 µg/mL, the activity of generated $SrFe_{12}O_{19}/TiO_2/ZnO$ increases marginally (3–4 mm for Salmonella enterica and 4 mm for Mycobacterium tuberculosis). With inhibition zones of 13 mm for Salmonella enterica and 15 mm for Mycobacterium tuberculosis at 20 µg/mL, moxifloxacin exhibits significantly improved antibacterial activity than a typical antibiotic. As the nanocomposite's concentration rises, its antibacterial activity gradually increases. A 4 mm zone against Salmonella enterica and a 5 mm zone against Mycobacterium tuberculosis are observed at 20 µg/mL. The inhibition zones for Salmonella enterica and Mycobacterium tuberculosis reach 9 mm and 11 mm, respectively, at 100 µg/mL. Although there is some antibacterial potential in the nanocomposite $SrFe_{12}O_{19}/TiO_2/ZnO$, moxifloxacin is still more effective in preventing bacterial growth at lower doses. As concentration rises, the nanocomposite's activity increases, suggesting that it may have antibacterial properties.

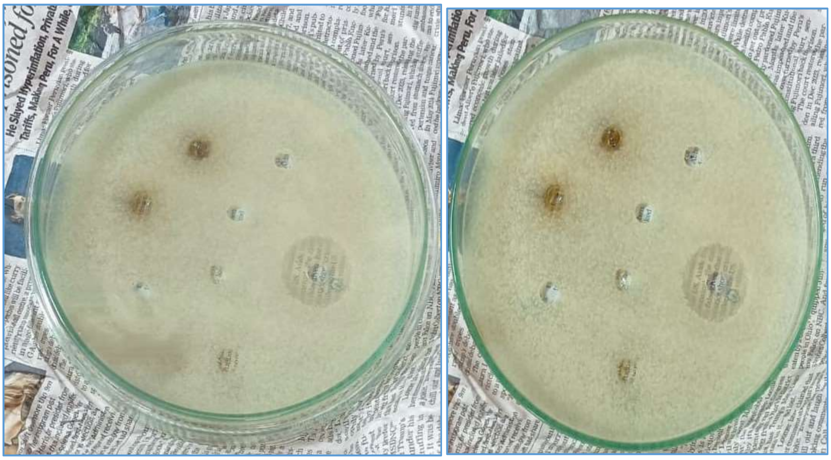

Fig.15. The antibacterial effect of nanoparticles including the inhibition zones

Table 1. Anti-bacterial activity of $SrFe_{12}O_{19}/TiO_2/ZnO$

Serial Number	Sample	Concentration {µg/mL}	*Salmonella enterica* (ATCC no: 35664) {Gram-positive} (mm)	*Mycobacterium tuberculosis* (ATCC no. 25618/H37RV) {Gram-negative} (mm)
A)	$SrFe_{12}O_{19}/TiO_2/ZnO$ synthesized	10	2	3
		50	2	3
		100	2	4
B)	Moxifloxacin $SrFe_{12}O_{19}/TiO_2/ZnO$ Nanocomposite	20	13	15
		20	4	5
		50	5	8
		100	9	11
C)	Moxifloxacin	20	15	17

4. Conclusion:

Recent photocatalytic studies on Malachite Green (MG) degradation highlight diverse nanomaterials designed for enhanced efficiency. Silver-manganese oxide nanoparticles exhibited 99% degradation under sunlight, optimized by pH and catalyst dosage. A La-doped SnO_2-CaO composite degraded MG under UV-visible light with high reusability. Graphene oxide and copper oxide composites achieved 90% efficiency under UV light, while $MoS_2/NiFe_2O_4$ nanocomposites delivered 98% degradation under visible light and were magnetically reusable. Further, ZnO-TiO_2 hybrids prepared via microwave-assisted synthesis showed rapid solar-driven MG degradation. Visible-light-active $BiFeO_3$/CuS nanohybrids achieved over 95% efficiency, combining synergistic properties of both materials. Additionally, nitrogen-doped carbon dots immobilized on TiO_2 improved MG degradation rates through enhanced light absorption. Metal-organic frameworks like ZIF-8 functionalized with TiO_2 also showcased excellent photodegradation results, demonstrating progress in advanced material designs for dye removal in wastewater in summary, $SrFe_{12}O_{19}/TiO_2$/ZnO trimetallic oxide nanoparticles were successfully synthesized, characterized, and evaluated for their photocatalytic degradation of Malachite Green and antibacterial activity. The nanoparticles exhibited a spherical shape with a particle size of 15–26 nm, and we confirmed their semiconductor properties with a bandgap of 2.29 eV. The photocatalyst achieved a 100% degradation efficiency of Malachite Green dye, widely used in textile and pharmaceutical industries, under solar irradiation. The antibacterial effectiveness of the nanoparticles was shown to be concentration-dependent. Characterization through UV-DRS, XRD, SEM, TEM, FTIR, and VSM confirmed that $SrFe_{12}O_{19}/TiO_2$/ZnO is a promising photocatalytic, recyclable, and stable nanocomposite.

5. Acknowledgment: In this research at the Andhra University of North Campus, the authors express their gratitude to Andhra University in Visakhapatnam, India's Advanced Analytical Laboratory for providing them with spectral analysis.

6. Declaration: The authors certify that no issue of interest is associated with this article's publication.

7. REFERENCES:

1.Muhammad Zahid, Nimra Nadeem, Muhammad Asif Hanif, Ijaz Ahmad Bhatti, Haq Nawaz Bhatti, and Ghulam Mustafa, Metal Ferrites and Their Graphene-Based Nanocomposites: Synthesis, Characterization, and Applications in Wastewater Treatment, 24 May 2019 Springer Nature, DOI: 10.1007/978-3-030-16439-3_10

2. Arun Karnwal, Tabarak Malik, Nano-revolution in heavy metal removal: engineered nanomaterials for cleaner water Sec. Water and Wastewater Management Volume 12 – 2024 https://doi.org/10.3389/fenvs.2024.1393694

3. Hayfa Alajilani, Abraheem Jamjoum, Khalid Umar, Rohana Adnan, Mohd. R. Razali, and Mohamad Nasir Mohamad Ibrahim Synthesis, Characterization, and Photocatalytic Activities of Graphene Oxide/metal Oxides Nanocomposites: A Review, Front Chem. 2021; 9: 752276 ,2021 Sep 21, Doi: 10.3389/fchem.2021.752276

.4. panel Marica Muscetta, Priyanka Ganguly, Laura Clarizia Solar-powered photocatalysis in water purification: applications and commercialization challenges, Volume 12, Issue 3, June 2024, 113073 Journal of Environmental Chemical Engineering, https://doi.org/10.1016/j.jece.2024.113073

5. Ehab A. Abdelrahman and Eida S. Al-Farraj Facile Synthesis and Characterizations of Mixed Metal Oxide Nanoparticles for the Efficient Photocatalytic Degradation of Rhodamine B and Congo Red Dyes, Nanomaterials 2022, 12, 3992. https://doi.org/10.3390/nano12223992

6. Jacques C, Vedrine, Review Heterogeneous Catalysis on Metal Oxides *Catalysts* 2017, *7*(11), 341; https://doi.org/10.3390/catal7110341

7. M. R. Dadfar S. A. Seyyed Ebrahimi S. M. Masoud Panah J Sol-Gel Synthesis and Characterization of SrFe12O19/TiO2 Nanocomposites Supercond Nov Magn (2015) 28:89–94 DOI 10.1007/s10948-014-2802-y

8. Asma S. Al-Wasidi and Ehab A. Abdelrahman, Functionalization of Strontium Ferrite Nanoparticles with Novel Chitosan–Schiff Base Ligand for Efficient Removal of Pb (II) Ions from Aqueous Media Inorganics 2024, 12, 148. https://doi.org/10.3390/inorganics12060148

9. Ehsan Naderi, Mahmoud Naseri, Dariush Souri The effect of SiO2 and TiO2 nanoparticles on physical properties of SrFe12O19 nanoparticle, Current Applied Physics. DOI: 10.1016/j.cap.2018.01.008

10. Abdullah G. Alanazi, Mohamed A. Habila, Zeid A. ALOthman and Ahmed-YacineBadjah-Hadj-Ahme Synthesis and Characterization of Zinc Oxide Nanoparticle Anchored Carbon as Hybrid Adsorbent Materials for Effective Heavy Metals Uptake from Wastewater *Crystals* 2024, *14*(5), 447;

11. Fatemeh Bavarsiha, Saeideh Dadashian, Mehdi Montazeri-Pour2, Fardin Ghasemy-Piranloo, Masoud Rajabi, Synthesis, characterization and photocatalytic efficiency of Fe3O4 /SiO2 /TiO2, SrFe12O19/SiO2 /TiO2 and Fe3O4 /SiO2 /ZnO core/shell/shell nanostructures, Processing and Application of Ceramics 16 [3] (2022) 291–301 https://doi.org/10.2298/PAC2203291B

12. Mritunjaya Parashar, Vivek Kumar Shukla, Ranbir Singh Metal oxide nanoparticles via sol-gel method: a review on synthesis, characterization, and applications. Journal of Materials Science: Materials in Electronics (2020) 31:3729–3749 https://doi.org/10.1007/s10854-020-02994-8

13. Guruprasad. Jaya Nayak, RajeshaGanalu, Shashikanth, ShareefrazaJ.Ukkund, Shamsuddin Ahmed, MajedAlSubih, and Saiful Islam, Studies on the Removal of Malachite Green from Its Aqueous Solution Using Water-Insoluble β-Cyclodextrin Polymers,
ACSOmega2024,9,10132−10145,https://doi.org/10.1021/acsomega.3c06504

14. Peter Olusakin Oladoye, Timothy Oladiran Ajiboye, Wycliffe Chisutia Wanyonyi, Elizabeth Oyinkansola Omotola, Mayowa Ezekiel Oladipo, Water Science and Engineering, Volume 16, Issue 3, September 2023, Pages 261-270 https://doi.org/10.1016/j.wse.2023.03.002

15. Somasekhar Ryali and Paul Douglas Sanasi, Graphene oxide–nano-titania composites for efficient photocatalytic degradation of indigo carmine, *Journal of the Chinese Chemical Society*., 65, 1423 (2018) https://doi.org/10.1002/jccs.201800154